

## Laboratory study of cross-polarized radar return under gale-force wind conditions

Yu Troitskaya<sup>a,b</sup>, V. Abramov<sup>c</sup>, A. Ermoshkin<sup>a</sup>, E. Zuikova<sup>a</sup>, V. Kazakov<sup>a</sup>, D. Sergeev<sup>a,b</sup>,  
A. Kandaurov<sup>a,b</sup>, and O. Ermakova<sup>a,b\*</sup>

<sup>a</sup>Geophysical Department, Institute of Applied Physics, Nizhny Novgorod 603950, Russian Federation; <sup>b</sup>Radiophysical Department, Lobachevsky State University of Nizhni Novgorod, Nizhny Novgorod 603950, Russian Federation; <sup>c</sup>Department of Radioastronomical Research of Cosmic Objects and Environments, Radiophysical Research Institute, Nizhny Novgorod 603950, Russian Federation

(Received 26 December 2014; accepted 25 February 2016)

This paper presents data of laboratory experiments on a high-speed wind-wave flume of the Institute of Applied Physics (Nizhny Novgorod, Russian Federation), which are devoted to the investigation of the X-band co-polarized and de-polarized radar return in a wide range of high wind speeds (from 8 to 40 m s<sup>-1</sup>). Microwave measurements were accompanied by the measurements of airflow and wave field parameters. Experiments showed that alternatively to the co-polarized return, the dependency of the de-polarized return on the wind speed does not saturate, although the growth rate decreases at wind speed exceeding 30 m s<sup>-1</sup>. Comparison of the experimental data with the composite-surface Bragg scattering model for the measured parameters of the wind and waves showed that the model is in agreement with measurements of microwave co-polarized return, but fails to describe the de-polarized radar return. The obtained dependency of de-polarized radar return was compared with the empirical geophysical model function based on collocated airborne and satellite data.

### 1. Introduction

The prevailing methods of monitoring wind speeds and directions over sea surface, which is vital for storm forecasting, employ satellite-based scatterometers (i.e. MetOp and, before 2009, QuikSCAT). The principle difficulty of the current wind speed retrievals using the dependence of microwave backscattering cross section on wind speed (geophysical model function (GMF)) (Hersbach 2010; Hersbach, Stoffelen, and de Haan 2007) is due to its saturation at winds exceeding 25 m s<sup>-1</sup> (Donnelly et al. 1999). Then, the accuracy of wind speed retrieval ceases for severe winds like in hurricanes and typhoons.

Recently, analysis of dual- and quad-polarization C-band radar return measured from satellite Radarsat-2 with co-located concomitant direct measurements of wind from oceanographic buoys National Data Buoy Center (Hwang, Zhang, Toporkov, et al. 2010; Zhang, Perrie, and He 2011; Vachon and Wolfe 2011; Zhang and Perrie 2012) suggested that the cross-polarized radar return does not saturate at higher winds and has a much higher sensitivity to the wind speed than co-polarized backscattering.

In a recent paper by Zadelhoff et al. (2014), the GMF for cross-polarized (vertical–horizontal (VH)) radar cross section (RCS) was derived on the basis of Radarsat-2 synthetic aperture radar (SAR) images acquired during hurricanes

---

\*Corresponding author. Email: o.s.ermakova@mail.ru

collocated with airborne wind measurements by Stepped-Frequency Microwave Radiometer (SFMR) (Uhlhorn et al. 2007) made by National Oceanic and Atmospheric Administration’s hurricane hunter flights. Since complete collocation of these data was not possible and time difference in flight legs and SAR images acquisition was up to 3 h, these two sets of data were compared in Zadelhoff et al. (2014) only statistically.

The main purpose of this paper is to investigate the functional dependence of cross-polarized RCS on the wind speed by a laboratory experiment. Since cross-polarized radar return is formed at small-scale features at the air–sea interface (short-crested waves, foam, sprays, etc.), which are well reproduced in laboratory conditions, then the approach based on laboratory experiment on radar scattering of microwaves at the water surface under hurricane wind looks appropriate.

## 2. Experimental facility

The experiments were performed in the wind-wave flume, which is the part of the large thermostratified tank of the Institute of Applied Physics (Troitskaya et al. 2012). The working straight part of the flume is 10 m and operating cross section is 0.40 m × 0.40 m; the axis velocity can be varied from 5 to 25 m s<sup>-1</sup>, which corresponds to  $U_{10}$  from 7 to 40 m s<sup>-1</sup>; here,  $U_{10}$  represents the equivalent 10-m wind speed.

### 2.1. Measurements of wind and waves

Parameters of the airflow in the turbulent boundary layer (friction velocity  $u^*$  and roughness height  $z_0$ ) were retrieved by velocity profiling and subsequent data processing based on self-similarity of the turbulent boundary layer in the flume described in Troitskaya et al. (2012). Then, the equivalent 10-m wind speed was calculated by definition:  $U_{10} = 2.5u^*\ln(10/z_0)$ .

The wind-wave field parameters in the flume were measured by three wire gauges positioned in the corners of an equal-side triangle with 2.5 cm side; the data sampling rate was 100 Hz. Three-dimensional frequency-wave-number spectra  $S(\omega, k, \theta)$  were retrieved from these data by the Fourier directional method (FDM) (Troitskaya et al. 2012); here  $k$  represents the wavenumber,  $\omega$  is the wave frequency, and  $\theta$  corresponds to the direction angle. Integrating  $S(\omega, k, \theta)$  over frequency yields wavenumber directional spectra  $S(k, \theta)$ . Integrating over  $\theta$  gives frequency spectra and the wavenumber spectra correspondingly. Saturation wavenumber spectrum of the waves at the working section for different wind speeds  $U_{10}$  are shown in Figure 1(a). For estimations of the cm-band wave spectra, data from another wave-gauge with the 0.8 cm base were used. Application of FDM yields the saturation wavenumber spectrum at  $1 \text{ cm}^{-1} < k < 4 \text{ cm}^{-1}$ , which can be approximated as follows:

$$B(k, \theta) = \frac{2}{\pi} \alpha k^\beta \cos^2 \theta, \quad (1)$$

where the dependence of  $\alpha$  and  $\beta$  on  $U_{10}$  are shown in Figure 1(b).

Also, the slope probability density function (PDF) for ‘long waves’ was obtained by comparing with the composite Bragg theory of microwave radar return according to Valenzuela (1978) and Plant (1990). When calculating the slope PDF of ‘long waves’ from experimental data (Figure 2), the dividing scale was set equal to three

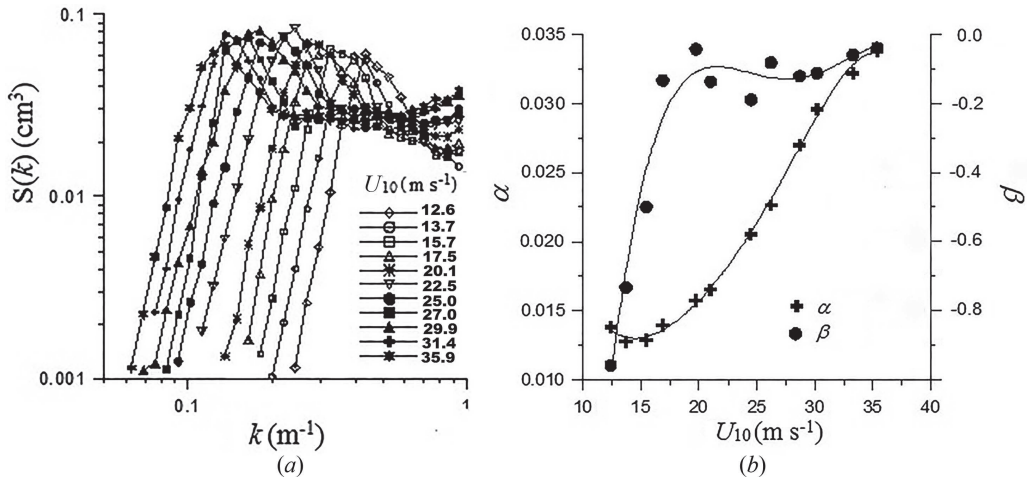


Figure 1. Saturation wavenumber spectrum of the waves at the working section for different wind speeds  $U_{10}$  (a), and dependencies of  $\alpha$  and  $\beta$  in Equation (1) on  $U_{10}$  (b).

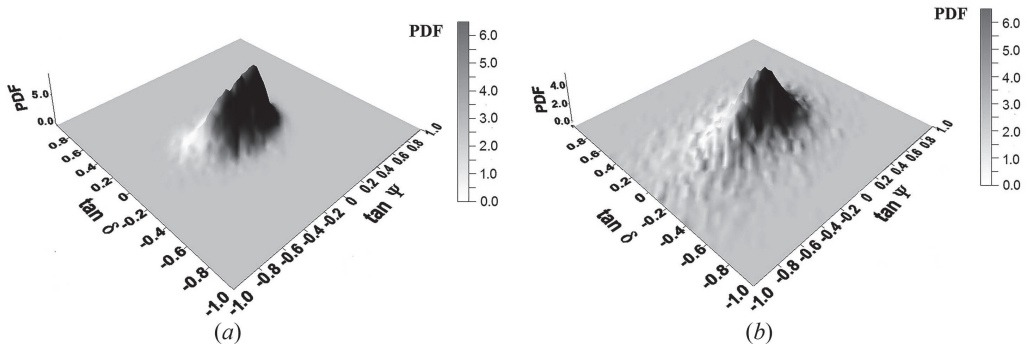


Figure 2. Slope probability density function (PDF) of large waves  $k < \frac{k_b}{3}$ ,  $k_b$  is the Bragg wavenumber. Wind speeds  $U_{10}$  are  $12.4 \text{ m s}^{-1}$  (a) and  $28.7 \text{ m s}^{-1}$  (b).

Bragg wavelengths. Note that the peculiarity of wind waves in this experiment was its high degree of nonlinearity and linear filtering of data was expected to lead to a strong distortion of the waveform. In this regard, for discrimination of the ‘long waves’, the empirical mode decomposition (EMD) (Huang et al. 1998) was implemented. Taking into account that time series of the water surface elevations are characterized by a high degree of intermittency (Huang, Shen, and Long 1999), the algorithm of Ensemble EMD was applied (Wu and Huang 2009), which allows avoiding the phenomenon of ‘mixing modes’. When constructing the slope PDF for ‘long waves’ from the original time series of water surface elevations, high-frequency intrinsic mode functions were subtracted in accordance with the criterion of the scale separation. Strong nonlinearity of the ‘long waves’ resulted, in particular, in marked difference of slope PDF from the Gaussian distribution.

## 2.2. Microwave measurements

Microwave measurements were carried out by a coherent Doppler X-band ( $\lambda = 3.2 \text{ cm}$ ) scatterometer with the consequent receive of linear polarizations. Antenna is an optimized

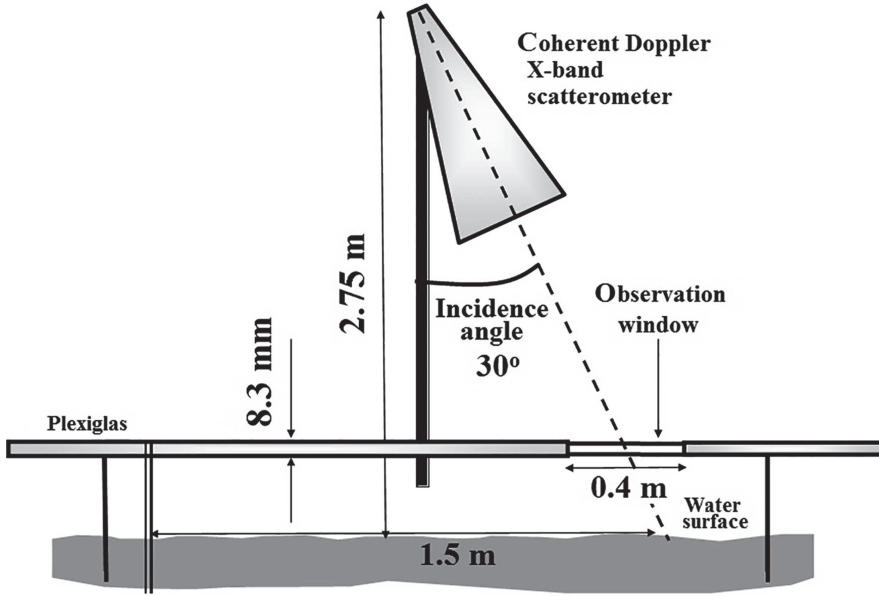


Figure 3. Principal scheme of the experimental set-up in the working section for microwave measurements.

pyramidal horn with square cross section  $224 \text{ mm} \times 224 \text{ mm}$  and a length of 680 mm, which is equipped with the orthomode transducer with isolation of polarizations of more than 40 dB; the beam width was  $9^\circ$ . The absolute value of the RCS of rough water surface was determined by comparing the scattered signal with the signal reflected from the reference reflector (calibrator) with the known value of the RCS – a metal ball-pendulum of 6 cm diameter.

Principal scheme of the experimental set-up in working section at a distance of 6 m from the inlet is shown in Figure 3.

The observation window was  $40 \text{ cm} \times 40 \text{ cm}$ , incidence angle was  $30^\circ$ , distance from the target was 3.16 m at the height 2.75 m from the water, and the thickness of the Plexiglas of the flume was 8.3 mm. To reduce the influence of reflections taken from the side lobes, the most ‘critical’ reflectors of the tank were covered with pieces of radio-absorbing material.

### 3. Results of experiments and geophysical model function

The dependencies of normalized radar cross section (NRCS)  $\sigma_0$  in linear units for four polarizations (horizontal transmit and horizontal receive (HH), vertical transmit and vertical receive (VV), horizontal transmit and vertical receive (HV), and vertical transmit and horizontal receive (VH)) are shown in Figure 4. One can see that the cross-polarized radar return is two orders lower than the co-polarized one and has higher sensitivity to the wind speed. Indeed, the cross-polarized RCS  $\sigma_{0VH}$  expressed in linear units at  $U_{10} < 25 \text{ m s}^{-1}$  grows proportionally to  $(U_{10})^2$ , while  $\sigma_{0VV}$  and  $\sigma_{0HH}$  expressed in linear units are proportional to  $(U_{10})^{1.5}$  at  $U_{10} < 22 \text{ m s}^{-1}$ . At wind speeds exceeding  $25 \text{ m s}^{-1}$ , the cross-polarized radar return growth slows down and becomes proportional to  $U_{10}$ , while  $\sigma_{0VV}$  and  $\sigma_{0HH}$  goes down proportionally to  $(U_{10})^{0.5}$  at  $U_{10} > 22 \text{ m s}^{-1}$ .

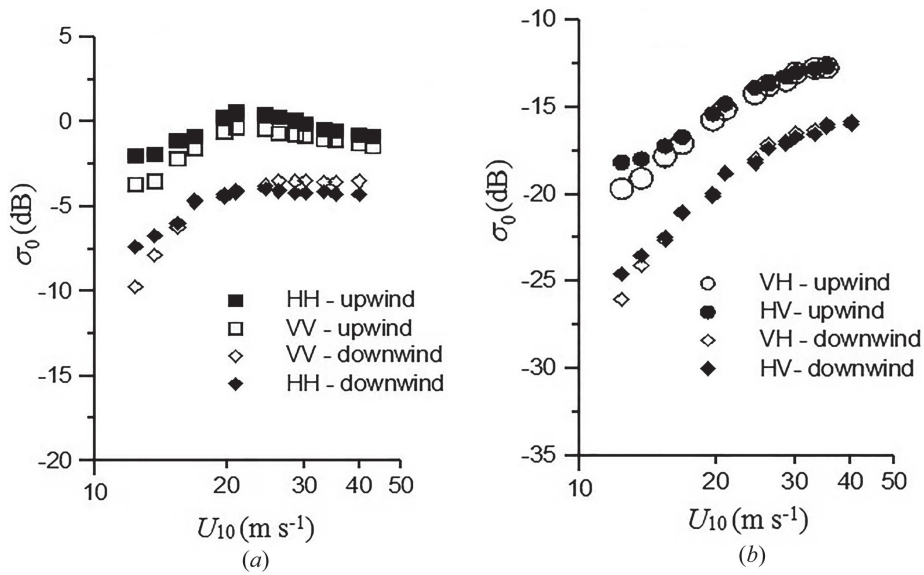


Figure 4. Co-polarized (a) and de-polarized (b) NRCS plotted against wind speed upwind and downwind looking, incidence angle is  $30^\circ$ .

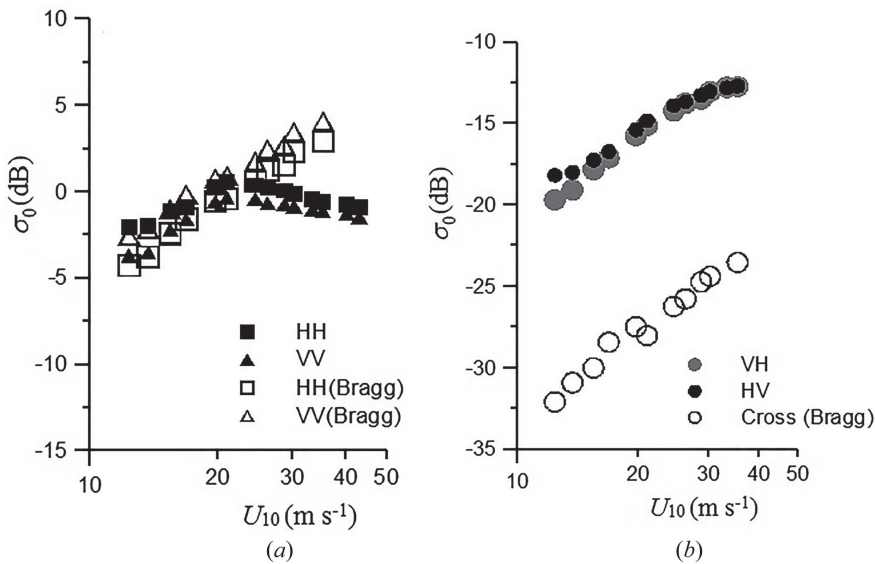


Figure 5. Comparison of measured co-polarized and cross-polarized radar cross sections and predictions of composition Bragg model.

In Figure 5, we compared measured  $\sigma_{0PQ}$  (here  $P$  and  $Q$  denotes different polarizations and equal to H or V) with the predictions of composite Bragg theory (Valenzuela 1978; Plant 1990), where the spectral density of surface waves and PDF for 'long waves' were taken from the measurements of the wave field. In this configuration of experimental set-up, the Bragg wave length was  $\lambda_b = 3.2$  cm and cut-off wave length was  $5\lambda_b$ .

The article by Valenzuela (1978) gives the following expressions for RCS on the co-polarization and cross-polarization:

$$\sigma_0(\theta_i)_{\text{HH}} = 4\pi k^4 \cos^4 \theta_i \left| \left( \frac{\alpha \cos \delta}{\alpha_i} \right)^2 g_{\text{HH}}(\theta_i) + \left( \frac{\sin \delta}{\alpha_i} \right)^2 g_{\text{VV}}(\theta_i) \right|^2 \times S(2k\alpha, 2k\gamma \sin \delta), \quad (2)$$

$$\sigma_0(\theta_i)_{\text{VV}} = 4\pi k^4 \cos^4 \theta_i \left| \left( \frac{\alpha \cos \delta}{\alpha_i} \right)^2 g_{\text{VV}}(\theta_i) + \left( \frac{\sin \delta}{\alpha_i} \right)^2 g_{\text{HH}}(\theta_i) \right|^2 \times S(2k\alpha, 2k\gamma \sin \delta), \quad (3)$$

$$\sigma_0(\theta_i)_{\text{HV}} = \sigma_0(\theta_i)_{\text{VH}} = 4\pi k^2 \cos^4 \theta_i \left( \frac{\alpha \sin \delta \cos \delta}{\alpha_i^2} \right)^2 |g_{\text{VV}}(\theta_i) - g_{\text{HH}}(\theta_i)|^2 \times S(2k\alpha, 2k\gamma \sin \delta), \quad (4)$$

where  $\theta_i = \cos^{-1}(\cos(\theta + \psi) \cos \delta)$  is the resultant angle of incidence;  $\psi$  is an angle in the plane of incidence and  $\delta$  is an angle in a plane perpendicular to the plane of incidence;  $\alpha_i = \sin \theta_i$ ,  $\alpha = \sin(\theta + \psi)$ ,  $\gamma = \cos(\theta + \psi)$  and  $g_{\text{VV}}, g_{\text{HH}}$  are the first-order scattering coefficients:

$$g_{\text{HH}}(\theta_i) = \frac{(\varepsilon_r - 1)}{\left[ \cos \theta_i + (\varepsilon_r - \sin^2 \theta_i)^{1/2} \right]^2}, \quad (5)$$

$$g_{\text{VV}}(\theta_i) = \frac{(\varepsilon_r - 1) [\varepsilon_r (1 + \sin^2 \theta_i) - \sin^2 \theta_i]}{\left[ \varepsilon_r \cos \theta_i + (\varepsilon_r - \sin^2 \theta_i)^{1/2} \right]^2}, \quad (6)$$

where  $\varepsilon_r$  is the relative dielectric constant of the ocean. Accordingly, the backscattering cross section per unit area of the sea is obtained from

$$\sigma_0^{\text{sea}}(\theta)_{PQ} = \int_{-\infty}^{+\infty} d(\tan \psi) \int_{-\infty}^{+\infty} d(\tan \delta) \sigma_0(\theta_i)_{PQ} p(\tan \psi, \tan \delta), \quad (7)$$

where  $p(\tan \psi, \tan \delta)$  is the joint probability density of slopes for the large-scale roughness of the ocean.

One can see that for co-polarized radar returns, the difference with the model is about 2–4 dB for wind speeds less than  $20 \text{ m s}^{-1}$  and it can be explained by our poor knowledge of the short-wave part of the spectrum. The difference increases at  $U_{10} > 20 \text{ m s}^{-1}$ , when the composed Bragg theory predicts growth of the NRCS with the wind speed, while the experimental results decrease. For cross-polarized return, the difference is about 8 dB, which means that some non-Bragg mechanisms (short-crested waves, foam, sprays, etc.) are responsible for the depolarization of the returned signal (Fois et al. 2014). It seems reasonable to compare the dependence of cross-polarized X-band RCS on 10-m wind speed obtained in laboratory conditions with the similar dependence obtained in Zadelhoff et al. (2014) from the field data for C-band RCS.

In Figure 6, we superimpose the laboratory X-band data with the distribution of all retrieved SFMR wind speeds versus collocated VH measurement points from nine hurricanes (Zadelhoff et al. 2014). One can see that the laboratory data follow the median

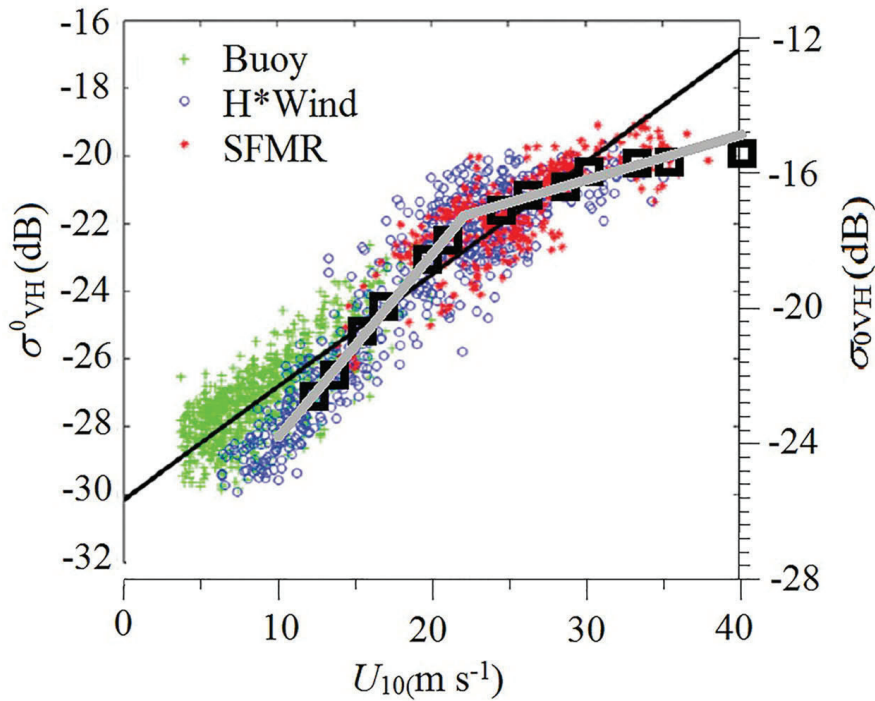


Figure 6. Distribution of all retrieved SFMR wind speeds versus collocated VH measurement points from nine hurricanes from Zadelhoff et al. (2014), H\*Wind from Zhang et al. (2014), and superimposed laboratory data (black squares).

of the field data with the constant bias 4–5 dB. Fitting the experimental data by polynomial curves gives the GMF obtained for incidence angle  $30^\circ$  and azimuth angle  $0^\circ$ . Best-fit line for X-band data gives

$$\sigma_{0VH}^X = \begin{cases} -29.2 \text{ dB} + 0.54U_{10}, & \text{for } 10 < U_{10} < 22, \\ -20.2 \text{ dB} + 0.13U_{10}, & \text{for } U_{10} > 22. \end{cases} \quad (8)$$

Taking into account the constant bias about 8 dB gives for C-band,

$$\sigma_{0VH}^C = \begin{cases} -37 \text{ dB} + 0.54U_{10}, & \text{for } 10 < U_{10} < 22, \\ -28 \text{ dB} + 0.13U_{10}, & \text{for } U_{10} > 22. \end{cases} \quad (9)$$

#### 4. Conclusion

Laboratory experiments directed to the investigation of co-polarized and cross-polarized X-band microwave radar return from the water surface at strong and hurricane wind were carried out. Parameters of airflow velocity (wind friction velocity and roughness height) and surface wind waves (spectra and PDF of slopes) in the laboratory facility were retrieved from simultaneous measurements. It was shown that alternatively to the co-polarized return, the dependency of the cross-polarized return on the wind speed is unambiguous, although the growth rate of RCS on wind speed decreases at wind speed exceeding  $30 \text{ m s}^{-1}$ .

We compared the dependency of the cross-polarized X-band RCS on wind speed obtained in laboratory with the similar dependency retrieved from Radarsat-2 SAR images

and collocated airborne SFMR wind measurements (Zhang and Perrie 2012; Zadelhoff et al. 2014). We found out that the laboratory data follow the median of the field data with the constant bias 4–5 dB. Based on laboratory data, an empirical GMF was suggested for retrieving wind speed up to 40 m s<sup>-1</sup> from cross-polarized microwave return, which is in good agreement with the direct measurements.

### Disclosure statement

No potential conflict of interest was reported by the authors.

### Funding

Microwave experiments and data processing (A. Ermoshkin, V. Abramov) were carried out under the financial support of the RSF (project 14-17-00667), wave measurements were supported by RFBR (projects 13-05-00865, 13-05-12093, 14-05-91767), and equipment was provided by grant from the Government of the Russian Federation (project code 11.G34.31.0048). Travel was supported by the research project ‘Air-Sea Interaction under Stormy and Hurricane Conditions: Physical Models and Applications to Remote Sensing’ (ASIST, Project No. 612610).

### References

- Donnelly, W. J., J. R. Carswell, R. E. McIntosh, P. S. Chang, J. Wilkerson, F. Marks, and P. G. Black. 1999. “Revised Ocean Backscatter Models at C and Ku Band under High-Wind Conditions.” *Journal of Geophysical Research: Oceans* 104 (C5): 11485–11497. doi:10.1029/1998JC900030.
- Fois, F., P. Hoogeboom, F. Le Chevalier, and A. Stoffelen. 2014. “Future Ocean Scatterometry at Very Strong Winds.” Geoscience and Remote Sensing Symposium (IGARSS), 2014 IEEE International, July 13–18, 3886–3889. doi:10.1109/IGARSS.2014.6947333
- Hersbach, H. 2010. “Comparison of C-Band Scatterometer CMOD5.N Equivalent Neutral Winds with ECMWF.” *Journal of Atmospheric and Oceanic Technology* 27: 721–736. doi:10.1175/2009JTECHO698.1.
- Hersbach, H., A. Stoffelen, and S. de Haan. 2007. “An Improved C-Band Scatterometer Ocean Geophysical Model Function: CMOD5.” *Journal of Geophysical Research* 112: C03006. doi:10.1029/2006JC003743.
- Huang, N. E., Z. Shen, and S. R. Long. 1999. “A New View of Nonlinear Water Waves: The Hilbert Spectrum 1.” *Annual Review of Fluid Mechanics* 31: 417–457. doi:10.1146/annurev.fluid.31.1.417.
- Huang, N. E., Z. Shen, S. R. Long, M. C. Wu, H. H. Shih, Q. Zheng, N.-C. Yen, C. C. Tung, and H. H. Liu. 1998. “The Empirical Mode Decomposition and the Hilbert Spectrum for Nonlinear and Non-Stationary Time Series Analysis.” *Proceedings of the Royal Society* 454A: 903–995. doi:10.1098/rspa.1998.0193.
- Hwang, P. A., B. Zhang, and W. Perrie. 2010. “Depolarized Radar Return for Breaking Wave Measurement and Hurricane Wind Retrieval.” *Geophysical Research Letters* 37: L01604. doi:10.1029/2009GL041780.
- Hwang, P. A., B. Zhang, J. V. Toporkov, and W. Perrie. 2010. “Comparison of Composite Bragg Theory and Quad-Polarization Radar Backscatter from RADARSAT-2: With Applications to Wave Breaking and High Wind Retrieval.” *Journal of Geophysical Research*. doi:10.1029/2009JC005995.
- Plant, W. J. 1990. “Bragg Scattering of Electromagnetic Waves from the Air/Sea Interface.” In *Surface Waves and Fluxes: Current Theory and Remote Sensing*, edited by G. L. Geernaert and W. J. Plant, 41–108. Dordrecht: Kluwer Academic Publishers. doi:10.1007/978-94-009-0627-3\_2.
- Troitskaya, Y. I., D. A. Sergeev, A. A. Kandaurov, G. A. Baidakov, M. A. Vdovin, and V. I. Kazakov. 2012. “Laboratory and Theoretical Modeling of Air-Sea Momentum Transfer under Severe Wind Conditions.” *Journal of Geophysical Research* 117: C00J21. doi:10.1029/2011JC007778.

- Uhlhorn, E. W., P. G. Black, J. L. Franklin, M. Goodberlet, J. Carswell, and A. S. Goldstein. 2007. "Hurricane Surface Wind Measurements from an Operational Stepped Frequency Microwave Radiometer." *Monthly Weather Review* 135: 3070–3085. doi:10.1175/MWR3454.1.
- Vachon, P. W., and J. Wolfe. 2011. "C-Band Cross-Polarization Wind Speed Retrieval." *IEEE Geoscience and Remote Sensing Letters* 8: 456–459. doi:10.1109/LGRS.2010.2085417.
- Valenzuela, G. R. 1978. "Theories for the Interaction of Electromagnetic and Oceanic Waves? A Review." *Boundary-Layer Meteorology* 13: 61–85. doi:10.1007/BF00913863.
- Wu, Z., and N. E. Huang. 2009. "Ensemble Empirical Mode Decomposition: A Noise-Assisted Data Analysis Method." *Advances in Adaptive Data Analysis* 1 (1): 1–41. doi:10.1142/S1793536909000047.
- Zadelhoff, G.-J., A. Stoffelen, P. W. Vachon, J. Wolfe, J. Horstmann, and M. Belmonte-Rivas. 2014. "Retrieving Hurricane Wind Speeds Using Cross-Polarization C-Band Measurements." *Atmospheric Measurement Techniques* 1 (7): 473–449. doi:10.5194/amt-7-437-2014.
- Zhang, B., and W. Perrie. 2012. "Cross-Polarized Synthetic Aperture Radar: A New Potential Measurement Technique for Hurricanes." *Bulletin of the American Meteorological Society* 93: 531–541. doi:10.1175/BAMS-D-11-00001.1.
- Zhang, B., W. Perrie, and Y. He. 2011. "Wind Speed Retrieval from RADARSAT-2 Quad-Polarization Images Using a New Polarization Ratio Model." *Journal of Geophysical Research* 116: C08008. doi:10.1029/2010JC006522.
- Zhang, B., W. Perrie, J. A. Zhang, E. W. Uhlhorn, and Y. He. 2014. "High-Resolution Hurricane Vector Winds from C-Band Dual-Polarization SAR Observations." *Journal of Atmospheric and Oceanic Technology* 31: 272–286. doi:10.1175/JTECH-D-13-00006.1.